Chapter 22
Tetrahedral Nanoclusters

Csaba L. Nagy, Katalin Nagy, and Mircea V. Diudea

Abstract Conserving the sp^2 hybridization of carbon atoms in tetrahedral arrangements is possible in both closed and opened nanostructures. Between the two classes, a structural relationship exists, and they can be easily transformed into each other to facilitate design of complex highly symmetric clusters. A classification of fullerenes with tetrahedral symmetry is here provided, and the corresponding zigzag and armchair tetrapodal nanotube junctions are discussed in detail.

22.1 Introduction

Shortly after the discovery of multi-walled carbon nanotubes, by Iijima, fullerene analogs with negative Gaussian curvature have been proposed (Scuseria 1992), where the pentagons in fullerenes are replaced with large non-hexagonal rings (e.g., heptagons) (Terrones and Terrones 2003). Highly symmetric nanotube junctions, as tetrahedral or octahedral units, can be assembled into networks resulting into infinite periodic minimal surfaces (Diudea and Nagy 2007). Such junctions could play an important role in the use of nanotubes in microelectronic devices (Terrones et al. 2002a, b, 2003).

There are software programs (Brinkmann et al. 2010; Schwerdtfeger et al. 2013) that can be used for the generation of fullerene cages. However, since a nanotube junction corresponds to a spanned fullerene, a systematic design of multiterminal junctions, with a given number of terminals and molecular symmetry, is required for the appropriate transforming of fullerenes.

C.L. Nagy (✉) • K. Nagy
Department of Chemistry, Faculty of Chemistry and Chemical Engineering, University of Babes-Bolyai, 400028 Cluj-Napoca, Romania
e-mail: nc35@chem.ubbcluj.ro

M.V. Diudea
Department of Chemistry, Faculty of Chemistry and Chemical Engineering, Babes-Bolyai University, Arany Janos Street 11, Cluj-Napoca RO-400028, Romania

A.R. Ashrafi, M.V. Diudea (eds.), *Distance, Symmetry, and Topology in Carbon Nanomaterials*, Carbon Materials: Chemistry and Physics 9,
DOI 10.1007/978-3-319-31584-3_22

Tetrahedral fullerenes with an open-shell electronic configuration should be very reactive; therefore, the ground state will have a lowered symmetry because of the first-order Jahn–Teller distortion (Jahn and Teller 1937). However, the topological symmetry could be achieved in the case of ions, heteroatom-doped analogs, or adducts. For example, the tetrahedral isomer of fullerene C_{40} has only two electrons in the triply degenerated frontier orbitals. The tetra-anion C_{40}^{4-}, the $C_{36}N_4$ nitrogen heteroanalog, and the $C_{40}H_4$ hydrogen adduct have a tetrahedral T_d configuration. It was found that the two electron-rich species are also highly aromatic, with nucleus-independent chemical shift (NICS) (Schleyer et al. 1996) values in the cage center -15.7 and -11.8 for C_{40}^{4-} and $C_{36}N_4$, respectively (Chen et al. 2001b).

Tetrahedral fullerene dication was also found to be highly stable (Diaz-Tendero et al. 2003, 2005). C_{52}^{2+} (T) has six adjacent pentagons and possesses lower energy than the isomers with only five adjacent pentagons, which reveals that the pentagon adjacency penalty rule (PAPR) (Campbell et al. 1996) does not necessarily apply to the charged fullerene cages. It is highly aromatic, as suggested by the -46.2 ppm negative NICS value (GIAO-6-31G*//B3LYP/6-31G*), and also very stable, as a consequence of the closed-shell electronic structure and nearly perfect sphericity.

The smallest tetrahedral fullerene has 28 carbon atoms and follows the $2(N+1)^2$ rule for spherical aromaticity (Hirsch et al. 2000). The ground state has an open-shell configuration with four singly occupied frontier orbitals; therefore, it is considered to be tetravalent with four dangling bonds localized on the triplet-pentagon fusion apices and prefers to encapsulate metal atom inside to form endohedral metallofullerenes $M@C_{28}$, as was observed in the gas-phase experiments (Guo et al. 1992). Upon reduction, the valence shell is completely filled, and the C_{28}^{4-} anion is highly aromatic, as predicted by -35.5 ppm (GIAO–SCF/6–31G*//B3LYP/6–31G*) NICS value at the cage center (Chen et al. 2001a). The heteroatom-substituted $C_{24}N_4$ also has a high delocalization of the electrons as indicated by the -27.8 ppm NICS at the cage center (Chen et al. 2001a).

By means of group theory, the formulas for the number of IR and Raman active modes, for all of the tetrahedral fullerenes, have been obtained (Cheng et al. 1999).

22.2 Tetrahedral Carbon Cages

According to the distribution of carbon atoms, the tetrahedral fullerenes can be classified as follows: (a) cages with no atoms along the symmetry axis, (b) fullerenes with four atoms lying on the threefold axis, and (c) cages with each of the threefold axes crossing two carbon atoms.

According to the number of carbon atoms (n), the tetrahedral fullerenes have been divided into three classes. It was found that the electronic structure, evaluated by means of Hückel theory, varies according to (1) $n = 12\ N$ in closed-shell fullerenes, (2) $n = 12N + 4$ in open shell, and (3) $n = 12N + 8$ in open-shell or pseudo-closed-shell electronic configuration, where N represents a nonnegative integer determined by group properties (Tang and Huang 1996).

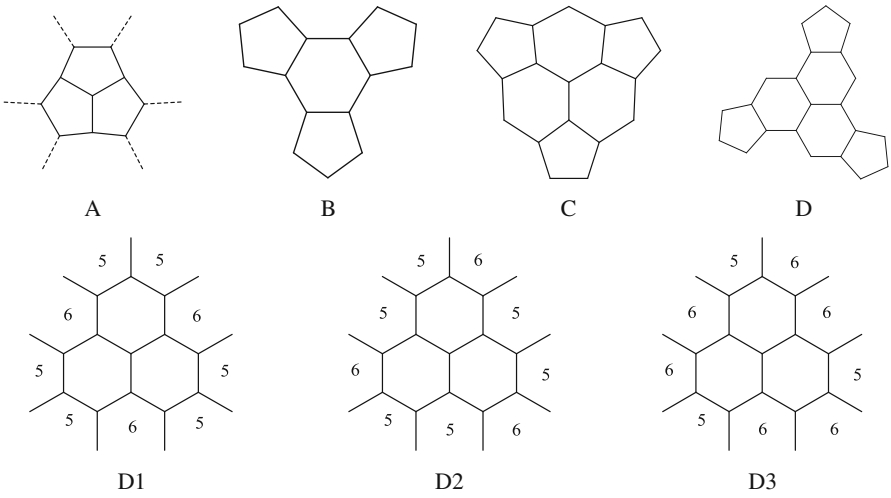

Fig. 22.1 Classification of the structural fragments decorating the tetrahedral carbon cages lying along the threefold symmetry axis. Some of the patterns have a common D fragment

The 12 fivefold rings are divided, by the molecular symmetry, into four equivalent fragments, each lying along one of the four threefold symmetry axis. The four structural patterns that have been identified are shown in Fig. 22.1. Pattern A is a directly fused pentagon triple, and, as a consequence, these fullerenes do not obey the isolated pentagon rule (IPR) (Manolopoulos and Fowler 1992). With the increase of the number of atoms, the geometry of such a structure will become polyhedral, resembling a tetrahedron, as the giant icosahedral fullerenes resemble an icosahedron (Noël et al. 2014). Fragment B, commonly known as the sumanene, has a hexagonal ring core, surrounded by alternating pentagonal and hexagonal faces (with one exception, C_{28}–T_d). All fullerenes with B structural motif on at least 60 carbon atoms obey the IPR, and some of them are leapfrog fullerenes (Dias 1993). The other two classes have a carbon atom core and have isolated pentagons within the fragment.

Notice that tetrahedral fullerenes must have two of these fragments, and accordingly they belong to two classes, e.g., in the case of the C_{40}–T_d fullerene, the C_3 axis crosses both an A and a B motif.

In the systematic built of all tetrahedral armchair [3,3] nanotube junctions by the transformation (spanning) of tetrahedral fullerene cages, it seems that a given junction can be derived from more than one cluster. The structural relationship between the different molecule series is listed in Table 22.1. Some of the fullerenes have icosahedral instead of tetrahedral symmetry (e.g., C_{20}, C_{60}, and C_{80}); however, they arise by applying the structural transformation used in the other cases. Empty cells in the table represent non-fullerene polyhedrons.

Geometry optimization followed by the calculation of harmonic vibrational frequencies was performed at the density functional level of theory (DFT) using the hybrid B3LYP functional and the standard polarized double-zeta 6-31G(d,p) basis set. Single point energy calculation results are summarized in Fig. 22.2, where the

Table 22.1 Classification of the tetrahedral fullerenes with respect to the structural fragment and the structural relationship with the corresponding tetrahedral armchair nanotube junction

#	Tetrahedral armchair [3,3] junction	Tetrahedral fullerenes			
		C_{n-8} (A)	C_{n-24} (B)	C_{n-32} (C)	C_{n-56} (D)
1	$Tj[3,3]_{52}^{4-}$–T	C_{44}–T	C_{28}^{4-}–T_d	–	–
2	$Tj[3,3]_{64}^{4-}$–T_d	C_{56}–T_d	C_{40}^{4-}–T_d	–	–
3	$Tj[3,3]_{76}^{4-}$–T	C_{68}–T	C_{52}^{4-}–T	C_{44}–T	C_{20}^{2+}–I_h
4	$Tj[3,3]_{84}$–T	C_{76}^{4-}–T	C_{60}–I_h	C_{52}^{4-}–T	C_{28}^{4-}–T_d
5	$Tj[3,3]_{100}^{4-}$–T_d	C_{92}–T_d	C_{76}^{4-}–T_d	C_{68}^{4-}–T_d	C_{44}–T
6	$Tj[3,3]_{108}$–T_d	C_{100}^{4-}–T_d	C_{84}–T_d	C_{76}^{4-}–T_d	C_{52}^{4-}–T
7	$Tj[3,3]_{112}^{4-}$–T	C_{104}–T	C_{88}^{4-}–T	C_{80}^{6-}–I_h	C_{56}–T_d
8	$Tj[3,3]_{124}^{4-}$–T	C_{116a}–T	C_{100}^{4-}–T	C_{92}–T	$C_{68}^{4-/0}$–T_d/T
9	$Tj[3,3]_{144}$–T_d	C_{136}^{4-}–T_d	C_{120}–T_d	C_{112}^{4-}–T_d	C_{88}^{4-}–T

For open-shell clusters, the ionic form is mentioned

total energy per atom and the HOMO–LUMO energy gap are plotted as a function of the number of carbon atoms. It can be observed that within series A, the charged fullerenes have very high energy gap values. The total energy per atom decreases with the cluster size. Within series B, the neutral structures show the highest stability according to the gap values, as these fullerenes have leapfrog structures.

22.2.1 C_{57} Multi-cage

The assembly of four C_{20} (I_h) fullerene cages results in a tetrahedral multi-cage with 57 carbon atoms having exclusively five-membered rings (Diudea and Nagy 2012, 2013). Each cage shares the core vertex, such as C_{57} can be considered as a tetrahedral sp^3 carbon hyper-atom, where the cages correspond to the hybrid orbitals. The framework of the structure consists of a centrohexaquinane core (shaded rings in Fig. 22.3 left), with all tetravalent atoms, enclosed by four acepentalene (triple fused pentagon) fragments. The unit can assemble into hyperstructures, including the classical network of the diamond and lonsdaleite. Because of the high percentage of pentagons, these structures were generically called diamond D_5 (Diudea et al. 2011, 2012).

C_{57} has an open-shell electronic configuration, and the neutral structure lowers the symmetry to D_{2d}. The reduced form achieves maximal symmetry, and all fivefold rings belonging to the acepentalene fragment are equivalent. The electron-rich multi-cage has aromatic pentagons with NICS values comparable to the ones predicted for the acepentalene dianion $C_{10}H_6^{2-}$, −9.34 and −9.53 ppm, respectively. Strain relief by partial or total hydrogenation of the sp^2 carbon atoms was theoretically evaluated (Diudea and Nagy 2012).

The core of the adamantane hyperstructure C_{158} (Fig. 22.3 right) is the tetrahedral C_{28} (T_d) carbon cage. In a larger network, the hexagons are shared between two C_{28} fullerenes.

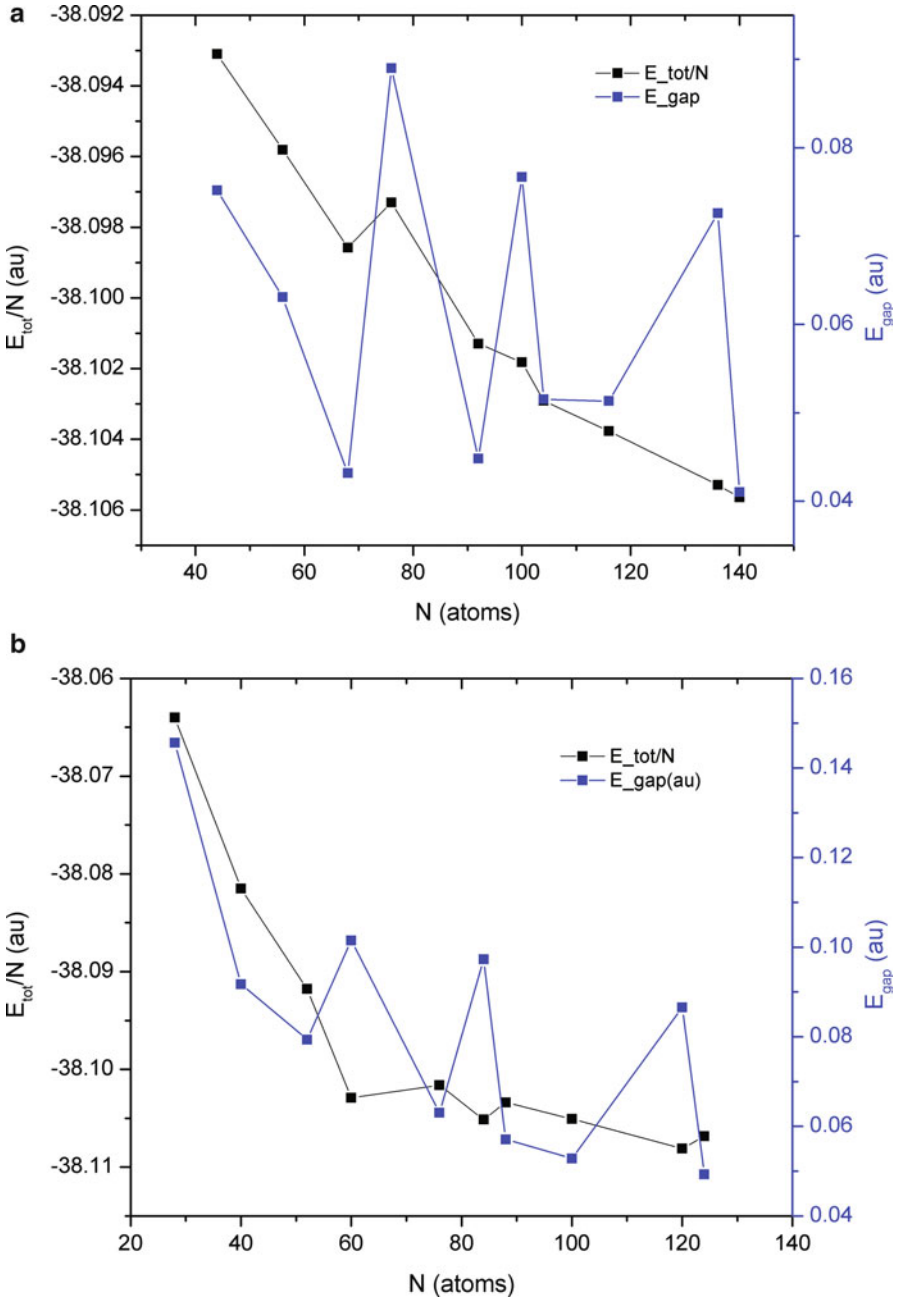

Fig. 22.2 Plot of the variation of the total energy per atom (E_{tot}/N in a.u.) and the HOMO–LUMO energy gap (E_{gap} in a.u.) as a function of the cluster size for the set of fullerenes in class A (*top*) and class B (*bottom*)

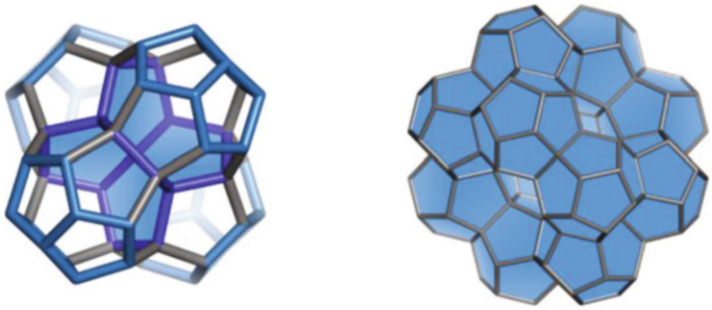

Fig. 22.3 Fragments of D_5 network: the C_{57} (T_d) multi-cage (*left*) and the corresponding hyper-adamantane C_{158} structure (*right*) (B3LYP/6-31G(d) optimized geometries)

22.3 Four-Terminal Nanotube Junctions

Multiterminal carbon nanotube junctions require, from a topological point of view, the insertion of structural defects in the hexagonal network of single-walled nanotubes. These defects are rings larger than hexagons which enables the assembly of individual nanotubes into a periodic network while preserving the sp^2 hybridization of the carbon atoms. In the following, tetrahedral zigzag and armchair nanotube junctions derived from fullerenes are presented, containing only heptagonal rings as defects.

22.3.1 Zigzag [3,0] Tetrahedral Junctions

The structure and stability of two tetrahedral three-terminal zigzag junctions consisting only of sp^2 covalent carbon atoms, $Tj[3,0]_{40}$ and $Tj[3,0]_{52}$, were investigated (Nagy et al. 2013) at the Hartree–Fock level of theory using the 6–31G(d,p) basis set as implemented in the Gaussian 09 software (Frisch et al. 2009). The structures were proven to be stable and possible to self-assemble in building diamond-like networks and hyper-dodecahedral architectures. Each opening of the junction fits a [3,0] zigzag single-walled carbon nanotube, found to be narrow-gap semiconductors (Borštnik et al. 2005). The junctions have been derived from the corresponding tetrahedral non-IPR fullerenes C_{44} (T) and C_{56} (T_d) by the removal of the core carbon atom from each of the triple directly fused pentagons. Both tetrapodal junctions incorporate only hexagonal rings; however, in a network, three octagonal rings are necessary at each connection to give a periodic surface with negative curvature (Romo-Herrera et al. 2007). The optimized geometries of the junctions are shown in Fig. 22.4.

The fullerenes C_{44} (T) and C_{56} (T_d) both have, according to the simple Hückel theory, pseudo-closed electron configuration, while the corresponding junctions are pseudo-open. As a consequence, the highest topological symmetry can be achieved

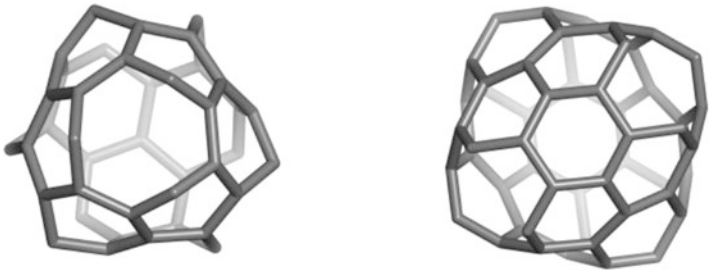

Fig. 22.4 HF/6-31G(d,p) optimized geometries of tetrahedral zigzag nanotube junctions: Tj[3,0]40–*T* (*left*) and Tj[3,0]$_{52}$–T_d (*right*)

Table 22.2 Energetic data for fullerenes and the corresponding tetrahedral junctions, at HF/6-31G(d,p) level of theory

Structure	E_{tot}/C atom (eV)	E_{gap} (eV)	SE (kcal/mol)
C_{44}–T	−37.852	6.595	12.73
Tj[3,0]$_{40}$–D_2	−38.021	6.681	5.80
Tj[3,0]$_{40}^{4-}$–T	−38.006	7.414	6.70
C_{52}–T_d	−37.854	5.505	10.65
Tj[3,0]$_{52}$–D_{2d}	−37.986	6.144	5.44
C_{60}–I_h	−37.864	7.418	8.256

by addition of some negative charges. The hexagonal framework of both junctions consists of four phenalene fragments. These motifs share one bond with each neighbor, in the case of the Tj[3,0]$_{40}$ junction, while in the case of Tj[3,0]$_{52}$, the fragments are disjointly separated by one bond. The 13-carbon phenalene cation and anion motif has a diatropic perimeter ring current, as in case of coronene (Balaban et al. 2010), predicted by the ipsocentric model (Cyrański et al. 2007).

Computational data, obtained using HF/6-31G(d,p) method, are listed in Table 22.2 (Nagy et al. 2013). The strain energy, evaluated according to POAV theory (Haddon 1990, 2001) is also included. It can be observed that the closed fullerenes show a higher strain in comparison to the opened junctions. The higher symmetry of the charged Tj[3,0]$_{40}^{4-}$ results in a higher strain when compared to the neutral lower symmetry structure.

As a consequence of the difference in the symmetry, the two tetrahedral junctions enable the building of two different networks by the assembly of the necessary number of units. In the case of the Tj[3,0]$_{40}$ dimer, the openings (terminals) are oriented in a staggered conformation, which leads to the assembly of a hyper-hexagon (chair conformation). Furthermore, a hyper-adamantane and hyper-diamantane can be obtained, as shown in Fig. 22.5. In contrast to this, from the Tj[3,0]$_{52}$ junction, a hyper-dodecahedron can be derived using 20 units, as a result of the occurrence of eclipsed terminals in the dimer (Fig. 22.6).

Details on the stability of some small structures built from the tetrapodal units can be found in Table 22.3, obtained at the HF/3–21G* level of theory

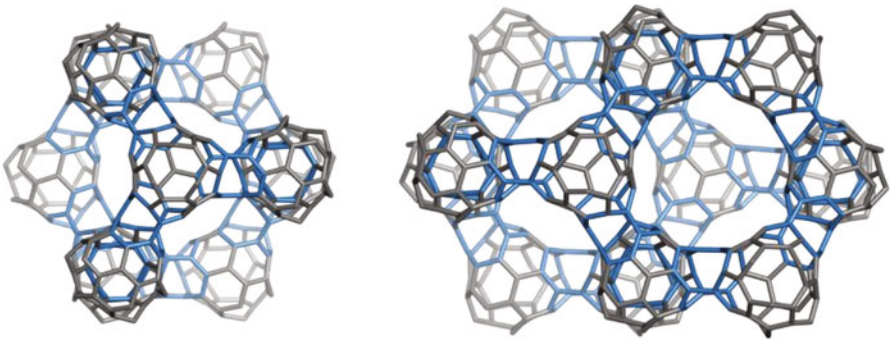

Fig. 22.5 The hyper-diamond substructures designed by Tj[3,0]$_{40}$ unit: hyper-adamantane Tj[3,0]$_{40}$_ada (*left*) and hyper-diamantane Tj[3,0]$_{40}$_dia (*right*)

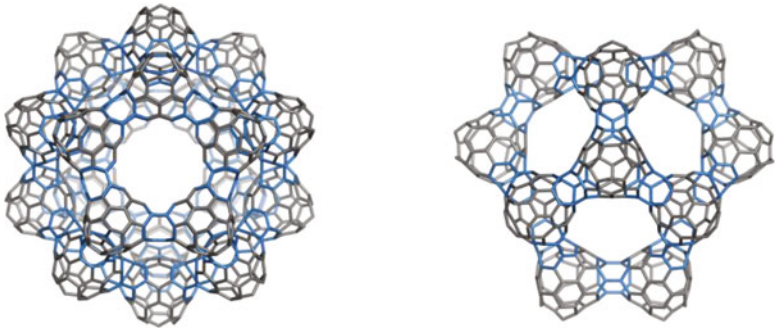

Fig. 22.6 The junction Tj[3,0]$_{52}$ enables the design of a hyper-dodecahedral architecture by joining 20 units (*left*). On the right side, a directly fused hyper-pentagon triple can be seen

Table 22.3 Computational data (HF/3–21G*) for smaller structures obtained by the assembly of tetrahedral nanotube junctions

Structure	E_{tot}/C atom (eV)	E_{gap} (eV)	SE (kcal/mol)
T_{j40}–dimer–C_3	−37.768	1.698	5.31
T_{j40}–trimer–C_2	−37.755	0.927	5.03
T_{j40}–hexagon–D_3	−37.728	7.382	4.57
T_{j52}–dimer–D_{3h}	−37.741	1.247	4.90
T_{j52}–trimer–C_{2v}	−37.731	0.891	4.67
T_{j52}–pentagon–D_{5h}	−37.711	6.755	4.25

(Nagy et al. 2013). Notice the overall structural relaxation increment observed in the strain energy with the increase in the number of joined units. According to HOMO–LUMO gap values, both hyper-ring structures have high kinetic stability.

In open multi-tori built up from u tetrapodal junction units, the genus of structure is calculated as $g = u + 1$, irrespective of the unit tessellation (Diudea and Szefler 2012). In closed unit multi-tori, the genus can be calculated by formula

Table 22.4 Calculation of the genus in opened and closed adamantane- and diamantane-like hyperstructures (multi-tori) by the Euler polyhedral formula and the number of repeat units

	v	e	f_6	f_8	f	$v-e+f$	g	u
Tj_{40}–ada	400	576	120	36	156	−20	11	10
Tj_{40}–dia	560	810	168	54	222	−28	15	14
Tj_{52}–hypDo	1040	1530	360	90	450	−40	21	20
	v	e	f_6	f_8	f_5	f	$v-e+f$	g
Tj_{52}–hypDo-closed	1060	1590	360	90	60	510	−20	11
Tj_{40}–ada-closed	416	624	120	36	48	204	−4	3
Tj_{40}–dia-closed	580	870	168	54	60	282	−8	5

$g = u - \sum_c (u_c \times c/2) + 1$ where c represents the number of closures per unit, while u_c is the number of units with c closures. Table 22.4 lists examples representing the proof of the above theorem (in agreement with the Euler formula) in both open and closed structures built up by the assembly of tetrapodal nanotube junctions (Nagy et al. 2013).

22.3.2 Armchair [3,3] Tetrahedral Junctions

Armchair nanotube junctions were systematically designed starting from the corresponding tetrahedral fullerenes; the structural relationship is listed in Table 22.1. The structural transformation involves removal and/or addition of atoms, also modification of the connectivity. The first nine elements of the [3,3] tetrahedral nanotube junctions are shown in Fig. 22.7, where the position of the heptagonal rings is marked in blue (B3LYP/6–31G(d,p) optimized geometries). According to the Euler formula, it is necessary to introduce 12 heptagons to obtain a genus 2 structure.

The orientation of the openings enables the construction of dimers in staggered conformation, resulting a hyper-diamond network. The hydrogenated units were studied using DFT method; the single point results are plotted in Fig 22.8. All structures were geometry optimized in the highest symmetry configuration; therefore, negative charges were included as necessary in the case of open-shell structures. Notice that the electronic shell of the junctions corresponds to that of the class B tetrahedral fullerenes.

The smallest junction includes only heptagonal rings and can be derived from fullerene C_{28} by replacing the pentagons with sevenfold rings. The junction having the hexagonal framework of C_{60} fullerene is $Tj[3,3]_{84}$ (T), which is the smallest leapfrog structure with isolated heptagonal rings.

In Fig. 22.8, one can observe that the stability ordering of the junctions is almost identical to the one observed in the case of class A fullerenes. The neutral tetrahedral junction $Tj[3,3]_{84}$ (T) showed the highest gap value indicating that the cluster has a high molecular stability.

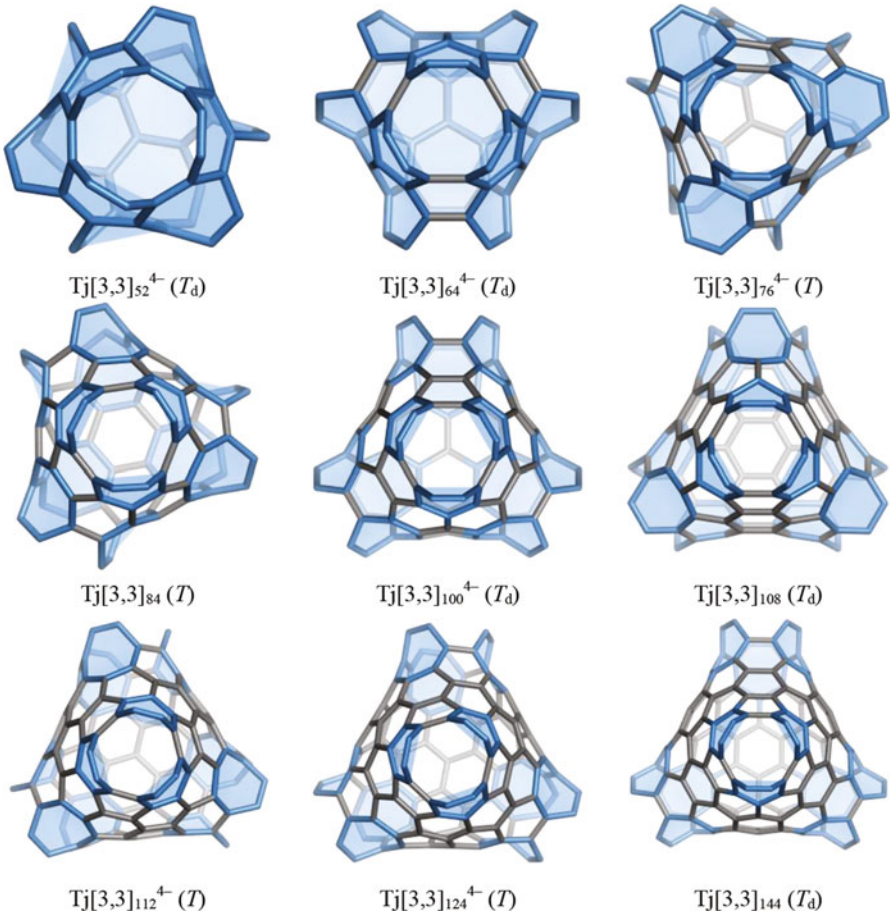

Fig. 22.7 DFT B3LYP/6–31G(d,p) optimized geometries of the armchair [3,3] carbon nanotube junctions. Position of the heptagonal rings is highlighted in *blue*

22.4 Conclusions

Tetrahedral fullerene cages have been classified according to the structural pattern found along the threefold symmetry axis and by the structural relationship with the corresponding nanotube junction. Armchair nanotube junctions having only heptagons and hexagons in the framework were built in a systematic way by spanning of the fullerenes. The supplied DFT results give an insight into the stability of tetrahedral nanoclusters. Diamond-like and dodecahedral hyperstructures were described from a topological point of view.

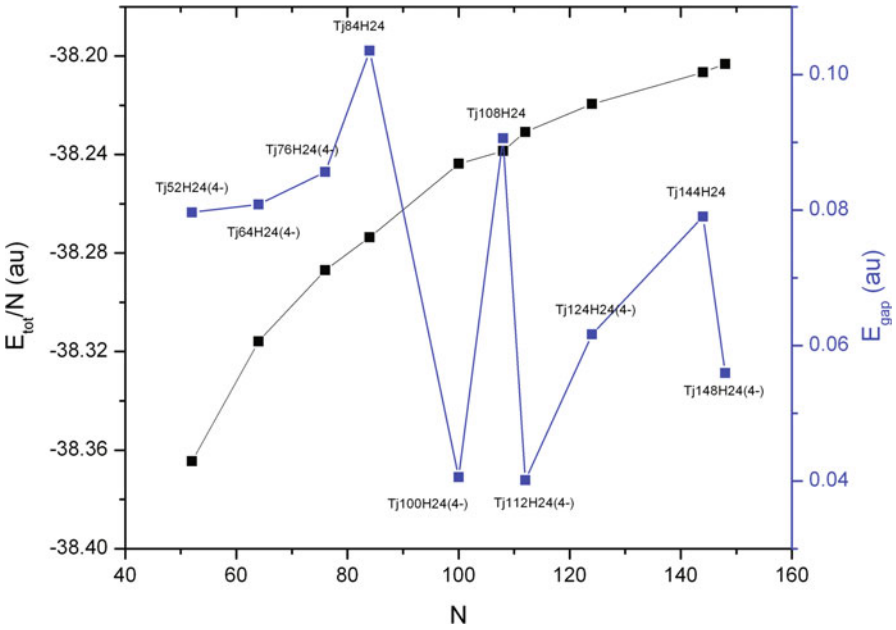

Fig. 22.8 Plot of the variation of the total energy per atom (E_{tot}/N in a.u.) and the HOMO–LUMO energy gap (E_{gap} in a.u.) as a function of the tetrahedral junction size

Acknowledgments CL Nagy acknowledges the financial support offered by the Babes-Bolyai University through Grant for Young Researchers GTC_34050/2013.

K Nagy acknowledges the financial support of the Sectorial Operational Program for Human Resources Development 2007–2013, co-financed by the European Social Fund, under the project number POSDRU/159/1.5/S/132400 with the title "Young successful researchers – professional development in an international and interdisciplinary environment".

References

Balaban AT, Bean DE, Fowler PW (2010) Patterns of ring current in coronene isomers. Acta Chim Slov 57:507–512

Borštnik U, Hodošček M, Janežič D, Lukovits I (2005) Electronic structure properties of carbon nanotubes obtained by density functional calculations. Chem Phys Lett 411:384–388

Brinkmann G, Delgado Friedrichs O, Lisken S, Peeters A, Van Cleemput N (2010) CaGe – a virtual environment for studying some special classes of plane graphs – an update. MATCH Commun Math Comput Chem 63:533–552

Campbell EEB, Fowler PW, Mitchell D, Zerbetto F (1996) Increasing cost of pentagon adjacency for larger fullerenes. Chem Phys Lett 250:544–548

Chen Z, Jiao H, Buhl M, Hirsch A, Thiel W (2001a) The $2(N+1)^2$ rule for spherical aromaticity: further validation. J Mol Model 7:161–163

Chen Z, Jiao H, Buhl M, Hirsch A, Thiel W (2001b) Theoretical investigation into structures and magnetic properties of smaller fullerenes and their heteroanalogues. Theor Chem Accounts 106:352–363

Cheng W, Li QS, Tang AC (1999) Vibrational spectra of tetrahedral fullerenes. J Mol Spectrosc 193:1–6

Cyrański MK, Havenith RWA, Dobrowolski MA, Gray BR, Krygowski TM, Fowler PW, Jenneskens LW (2007) The phenalenyl motif: a magnetic chameleon. Chem Eur J 13:2201–2207

Diaz-Tendero S, Alcami M, Martin F (2003) Theoretical study of ionization potentials and dissociation energies of C_n^{q+} fullerenes ($n = 50–60$, $q = 0$, 1 and 2). J Chem Phys 119:5545–5557

Diaz-Tendero S, Martin F, Alcami M (2005) Structure and electronic properties of fullerenes C_{52}^{q+}: is C_{52}^{2+} an exception to the pentagon adjacency penalty rule? ChemPhysChem 6:92–100

Diudea MV, Nagy CL (2007) Periodic nanostructures. Springer, Dordrecht

Diudea MV, Nagy CL (2012) C_{20}-related structures: diamond D_5. Diam Relat Mater 23:105–108

Diudea MV, Nagy CL (2013) Diamond D_5. In: Diudea MV, Nagy CL (eds) Diamond and related nanostructures, vol 6, Carbon materials: chemistry and physics. Springer, Dordrecht, pp 91–106

Diudea MV, Szefler B (2012) Nanotube junctions and the genus of multi-tori. Phys Chem Chem Phys 14:8111–8115

Diudea MV, Nagy CL, Ilic A (2011) Diamond D_5, a novel class of carbon allotropes. In: Putz MV (ed) Carbon bonding and structures, vol 5, Carbon materials: chemistry and physics. Springer, Dordrecht, pp 273–289

Diudea MV, Nagy CL, Bende A (2012) On diamond D_5. Struct Chem 23:981–986

Frisch MJ, Trucks GW, Schlegel HB, Scuseria GE, Robb MA, Cheeseman JR, Scalmani G, Barone V, Mennucci B, Petersson GA, Nakatsuji H, Caricato M, Li X, Hratchian HP, Izmaylov AF, Bloino J, Zheng G, Sonnenberg JL, Hada M, Ehara M, Toyota K, Fukuda R, Hasegawa J, Ishida M, Nakajima T, Honda Y, Kitao O, Nakai H, Vreven T, Montgomery JA, Peralta JE, Ogliaro F, Bearpark M, Heyd JJ, Brothers E, Kudin KN, Staroverov VN, Kobayashi R, Normand J, Raghavachari K, Rendell A, Burant JC, Iyengar SS, Tomasi J, Cossi M, Rega N, Millam NJ, Klene M, Knox JE, Cross JB, Bakken V, Adamo C, Jaramillo J, Gomperts R, Stratmann RE, Yazyev O, Austin AJ, Cammi R, Pomelli C, Ochterski JW, Martin RL, Morokuma K, Zakrzewski VG, Voth GA, Salvador P, Dannenberg JJ, Dapprich S, Daniels AD, Farkas Ö, Foresman JB, Ortiz JV, Cioslowski J, Fox DJ (2009) Gaussian 09, revision A.1. Gaussian Inc, Wallingford

Guo T, Diener MD, Chai Y, Alford MJ, Haufler RE, McClure SM, Ohno T, Weaver JH, Scuseria GE, Smalley RE (1992) Uranium stabilization of C_{28}: a tetravalent fullerene. Science 257:1661–1664

Haddon RC (1990) Measure of nonplanarity in conjugated organic molecules: which structurally characterized molecule displays the highest degree of pyramidalization? J Am Chem Soc 112:3385–3389

Haddon RC (2001) Comment on the relationship of the pyramidalization angle at a conjugated carbon atom to the σ bond angles. J Phys Chem A 105:4164–4165

Hirsch A, Chen Z, Jiao H (2000) Spherical aromaticity in I_h symmetrical fullerenes: the $2(N + 1)^2$ rule. Angew Chem Int Ed 39:3915–3917

Jahn H, Teller E (1937) Stability of polyatomic molecules in degenerate electronic states. I. Orbital degeneracy. Proc R Soc A 161:220–235

Manolopoulos DE, Fowler PW (1992) Molecular graphs, point groups, and fullerenes. J Chem Phys 96:7603–7614

Nagy K, Nagy CL, Tasnadi E, Katona G, Diudea MV (2013) Hyper-diamonds and dodecahedral architectures by tetrapodal carbon nanotube junctions. Acta Chim Slov 60:1–4

Noël Y, De La Pierre M, Zicovich-Wilson CM, Orlando R, Dovesi R (2014) Structural, electronic and energetic properties of giant icosahedral fullerenes up to C6000: Insights from an ab initio hybrid DFT study. Phys Chem Chem Phys 16:13390–13401

Ray Dias J (1993) Fullerenes to benzenoids and the leapfrog algorithm. Chem Phys Lett 204:486–490

Romo-Herrera JM, Terrones M, Terrones H, Dag S, Meunier V (2007) Covalent 2D and 3D networks from 1D nanostructures: designing new materials. Nano Lett 7:570–576

Schleyer PVR, Maerker C, Dransfeld A, Jiao H, Van Eikema Hommes NJR (1996) Nucleus-independent chemical shifts: a simple and efficient aromaticity probe. J Am Chem Soc 118:6317–6318

Schwerdtfeger P, Wirz L, Avery J (2013) Program fullerene – a software package for constructing and analyzing structures of regular fullerenes, version 4.4. J Comput Chem 34:1508–1526

Scuseria GE (1992) Negative curvature and hyperfullerenes. Chem Phys Lett 195:534–536

Tang AC, Huang FQ (1996) Electronic structures and stability rules of tetrahedral fullerenes. Chem Phys Lett 258:562–573

Terrones H, Terrones M (2003) Curved nanostructured materials. New J Phys 5:126.1–126.37

Terrones M, Banhart F, Grobert N, Charlier JC, Terrones H, Ajayan PM (2002a) Molecular junctions by joining single-walled carbon nanotubes. Phys Rev Lett 89:075505/1–075505/4

Terrones M, Charlier JC, Banhart F, Grobert N, Terrones H, Ajayan PM (2002b) Towards nanodevice fabrication: joining and connecting single-walled carbon nanotubes. New Diamond Front Carbon Technol 12:315–323

Terrones M, Banhart F, Hernández E, Grobert N, Charlier JC, Terrones H, Ajayan PM (2003) In-situ welding of single-walled carbon nanotubes and melting of encapsulated metal clusters in carbon shells: theory and experiment. Microsc Microanal 9:320–321